RESEARCH PAPER

Theoretical Prediction of a Phase Diagram for Solid Dispersions

Bin Tian • Xiaoyan Wang • Yuanyuan Zhang • Keru Zhang • Yu Zhang • Xing Tang

ABSTRACT

Purpose To predict the temperature-composition phase diagram of solid dispersions (SDs) through theoretical approaches using cinnarizine-Soluplus® SD as a model system and evaluate the predicted results.

Methods A complete phase diagram of cinnarizine-Soluplus® SD, including the solubility curve, miscibility curve and glass transition temperature curve, was constructed on the basis of the solid–liquid equilibrium (SLE) equation, Florry-Huggins (F-H) theory and Fox equation. Cinnarizine-Soluplus® SDs with different drug loadings were prepared by hot melt extrusion. The extrudates and corresponding physical mixtures were analyzed to check the predicted results.

Results The experimental data revealed a solubility of 7.9 wt% at 110°C and a miscibility level of 65 wt% at room temperature, which were both consistent with predicted values.

Conclusions The predicted phase diagram agrees well with the experimental results for the non-polar components which mainly interact through dispersion forces, thus facilitating the formulation design of SDs.

KEY WORDS miscibility · phase diagram · solid dispersion · solubility

INTRODUCTION

SDs have been proved to be one of the most promising strategies to enhance the solubility, dissolution and bioavailability of poorly water soluble drugs (1). However, the formulation design of SDs is still a great challenge for pharmaceutical scientists. It has been demonstrated that the solubility of a

B. Tian • X. Wang • Y. Zhang • K. Zhang • Y. Zhang • X. Tang (✉)
Department of Pharmaceutics Science, Shenyang Pharmaceutical
University, Wenhua Road 103, Shenyang 110016, Liaoning Province
People's Republic of China
e-mail: tanglab@126.com

crystalline drug in an amorphous polymer and the miscibility of a drug and a polymer are two key parameters for designing an optimal formulation (2,3). For a given drug-polymer binary system, the solubility and miscibility provide an important basis for the selection of a drug loading, which is related to the physical stability of SDs. The solubility defines the maximum drug loading for thermodynamically stable SDs, in which the drugs exist as molecularly dispersed compounds and will not undergo phase separation or crystallization during storage (4). On the other hand, the miscibility determines the upper limit of the drug loading for a metastable SD, because a higher drug loading will lead to spontaneous phase separation followed by drug crystallization, which would negate the advantages of SDs (2). Finally, for SDs with a drug loading between the solubility and miscibility, drugs disperse as amorphous molecular aggregates in the polymer matrix (5), and the SDs can maintain their amorphous status both thermodynamically and kinetically within a selected period of time (2). In addition, the glass transition temperature (T_g) is another critical parameter for SDs. As a demarcation between high and low molecular mobility, T_g can be used to predict the physical stability and select the proper storage temperature for SDs (6). However, it should be noted that the real T_gs of SDs can be lower than the predicted values due to the moisture absorption. The water can decrease the T_gs of SDs significantly as an plasticizing agent, and cause physical instability (7). As a result, the humidity must be taken into consideration when selecting storage conditions for SDs.

The solubility curve, miscibility curve and T_g curve (i.e., solubility, miscibility and T_g at different temperatures or compositions) allow the construction of a temperature-composition phase diagram, which provides valuable information facilitating the formulation design and product manufacturing of SDs (2,3,8). Consequently, it is highly desirable to establish a phase diagram for a drug-polymer binary system. However, due to the high viscosity of polymers, especially at temperatures below their T_g, the time required to

reach solubility equilibrium is rather long, making it a challenge to determine the drug-polymer solubility and miscibility at a variety of temperatures (4,9,10). Accordingly, in such cases, theoretical prediction is favored (11–13). Indeed, it has been reported that a phase diagram can be obtained by a theoretical approach according to F-H theory (3,8). In this theory, binodal and spinodal curves are thermodynamically defined (14,15). The binodal curve represents the phase boundary, outside of which a single phase is formed. On the other hand, the spinodal curve is the limit of metastability. At any point inside the spinodal curve, a spontaneous phase separation called spinodal decomposition occurs. This process is barrier-free, and can be initiated by any small composition fluctuation. While in the region between these two curves, the drug-polymer system is metastable, because large fluctuations are needed to overcome the nucleation barrier to initiate the phase separation. As a result, the binodal and spinodal curves correspond to the solubility and miscibility curves respectively. Compared with the solubility and miscibility, the determination of T_g is feasible, and can be performed by a wide range of techniques, such as differential scanning calorimetry (DSC), and dynamic mechanical analysis (DMA) (16). Moreover, T_g can also be predicted using equations as a function of composition (16–18).

Although the phase diagrams of SDs have been predicted theoretically, it is still unclear whether the predicted results could agree with the practical ones. In order to investigate this issue, cinnarizine (CIN)-Soluplus® SD prepared using the hot melt extrusion technique was selected as a model system in present work. The constructed temperature-composition phase diagram was evaluated by comparing the predicted results with the experimental data at a quantitative level. In addition, the variation in the form of drugs dispersed in polymers with the increased drug loading as well as the mixing level of the drug and polymer was also discussed.

MATERIALS AND METHODS

Materials

CIN was purchased from Shanghai Xiandai Hasen Pharma Ltd. Co. (Shangqiu, China) and used as received. Soluplus® (polyethylene glycol-polyvinyl caprolactam-polyvinyl acetate grafted copolymer) was a gift from BASF (Germany) and was milled before use (finer particles passing through the 100 mesh screen were collected). All other reagents were of analytical grade. The chemical structures of cinnarizine and Soluplus® are given in Fig. 1.

Prediction of the Solubility Curve

From a thermodynamic point of view, when the crystalline drug is in equilibrium with the dissolved drug, a saturated solution is formed. If the polymer is considered a solvent, then the solubility of a crystalline drug in a polymer could be calculated using the SLE equation:

$$\ln x_{drug} = \frac{\Delta H fus}{RT_m}\left(1-\frac{T_m}{T}\right)-\ln\gamma_{drug} \tag{1}$$

Where x_{drug} is the mole fraction of the dissolved drug, γ_{drug} is the activity coefficient, ΔH_{fus} is the heat of melting, R is the gas constant, T_m is the melting temperature and T is the temperature of the two phases of drug in equilibrium (19,20).

Apart from the melting temperature and the heat of melting of the drug which can be obtained by DSC, the activity coefficient of the drug is required to solve Eq. (1). Estimation of the activity coefficient of the drug was made on the basis of the extended Hansen model (20,21):

$$\ln\gamma_{drug} = \frac{Vdrug}{RT}\left\{\left(\delta_d^{drug}-\overline{\overline{\delta}}d\right)^2+0.25\left[\left(\delta_p^{drug}-\overline{\overline{\delta}}p\right)^2+\left(\delta_h^{drug}-\overline{\overline{\delta}}h\right)^2\right]\right\} \tag{2}$$
$$+\ln\frac{Vdrug}{\overline{V}}+1-\frac{Vdrug}{\overline{V}}$$

Where V is the molar volume, δ is the Hansen solubility parameter, $\overline{\delta}$ is the molar volume weighted Hansen solubility parameter, and $\overline{V}$ is the mixture volume. The subscripts d, p, and h stand for dispersion forces, polar interaction, and hydrogen bonding, respectively.

The mixture volume and molar volume weighted Hansen solubility parameter can be calculated using the following equations:
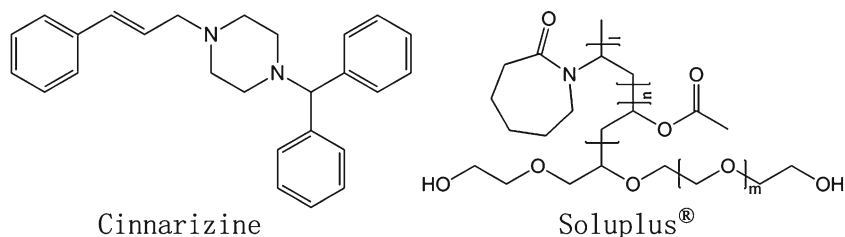
$$\overline{\overline{\delta}}=\sum_{k=1}^{n}\phi_k\delta_k \tag{3}$$

$$\phi_k=\frac{x_kV_k}{\overline{V}} \tag{4}$$

$$\overline{V}=\sum_{k=1}^{n}x_kV_k \tag{5}$$

$$V_k=\frac{M_k}{\rho_k} \tag{6}$$

Fig. 1 Chemical structures of cinnarizine and Soluplus®.

Cinnarizine   Soluplus®

Where ϕ is the volume fraction, x is the mole fraction, M is the molecular weight, ρ is the density, and the subscript k denotes the different components of the mixture.

The parameters needed for calculation of the solubility of the drug in the polymer at different temperatures are listed in Table I, and these were determined experimentally or taken from the literature.

Prediction of the Miscibility Curve

As stated previously, the miscibility curve corresponds to the spinodal curve, which can be predicted based on the F-H theory. For a drug-polymer binary system, the Gibbs free energy of mixing is described by Eq.(7) (3,8):

$$\Delta Gmix = RT\left[\phi\ln\phi + \frac{1-\phi}{m}\ln(1-\phi) + \chi\phi(1-\phi)\right] \qquad (7)$$

Where R is the gas constant, T is the absolute temperature, ϕ is the volume fraction of the drug, m is the number of lattice sites (defined here as the volume of a drug molecule) occupied by a polymer chain and χ is the drug-polymer interaction parameter.

The numbers of lattice sites occupied by a polymer chain and the drug-polymer interaction parameter can be calculated from Eqs. (8) and (9) respectively:

$$m = \frac{Mpolymer/\rho polymer}{Mdrug/\rho drug} \qquad (8)$$

$$\chi = \frac{v\left(\delta_{drug}-\delta_{polymer}\right)^2}{RT} \qquad (9)$$

Where v is the volume of a lattice site (i.e. volume of the drug).

The spinodal curve can be found by setting the second derivative of the free energy to zero and expressed as Eq. (10).

$$T_s = \frac{2v\left(\delta_{drug}-\delta_{polymer}\right)^2}{R} \cdot \frac{1}{\frac{1}{\phi} + \frac{1}{m(1-\phi)}} \qquad (10)$$

The parameters required for the estimation of the miscibility curve (i.e. spinodal curve) are shown in Table I.

Prediction of the T_g Curve

A series of equations have been proposed to estimate the T_g of a binary system (16–18). In this study, the Fox equation was used (24).

$$\frac{1}{Tg} = \frac{Wdrug}{Tg, drug} + \frac{1-Wdrug}{Tg, polymer} \qquad (11)$$

Where W_{drug} is the weight fraction of the drug.

Preparation of Physical Mixtures

CIN and Soluplus® were weighed accurately and manually mixed using a mortar and pestle to prepare the physical mixtures used for the DSC, PXRD, and FTIR measurements. The drug concentrations of the samples were 10, 20, 35, 50, and 65% w/w.

Preparation of Solid Dispersions

SDs were prepared by the hot melt extrusion technique with 10, 20, 35, 50, and 65% w/w CIN (denoted by SD-10, SD-20, SD-35, SD-50 and SD-65%). CIN and Soluplus® were premixed (batch size of 200 g) and fed into the hopper of a co-rotating twin-screw extruder TE-20 (Coperion Keya Co., China). The materials were passed through the entire barrel consisting of four heated zones, at temperatures of 100, 120, 120 and 120°C from feeder to die. The feeding rate and the screw rate were both fixed at 3 Hz. The extrudates were collected after cooling at ambient temperature, milled with a laboratory cutting mill and stored in a desiccator at room temperature. The amorphous CIN was also prepared by melting and subsequent rapid cooling.

DSC Measurements

The DSC measurements were performed using a DSC 1 differential scanning calorimeter (Mettler Toledo, Switzerland) equipped with a refrigerated cooling system. Samples

Table I Data used for Calculation of the Solubility and Activity Coefficient of CIN

Substance	M (g/mol)	Density (g/cm³)	Heat of Melting (J/mol)	Molar volume (cm³/mol)	Melting point (K)	Solubility parameters[d] (Mpa$^{1/2}$)			
						δ_d	δ_p	δ_h	δ
CIN	368.52	1.13[a]	37670.11[b]	326.12[d]	391.4[b]	20.35	5.4	5.75	21.8
Soluplus®[c]	118,000	1.20	–	98,333	–	17.4	0.3	8.6	19.4

[a] Taken from the literature [22]

[b] Experimentally determined using DSC

[c] Data on Soluplus® were taken from the literature [20]

[d] Solubility parameters and molar volume of CIN were calculated as described in the literature [23]

(approximately 4 mg, accurately weighed) were placed in hermetically sealed aluminum pans for analysis. A pin hole was made in the lid to allow the escape of moisture. Nitrogen at a flow rate of 80 mL/min was used as the purge gas. The instrument was calibrated for temperature and enthalpy using indium and zinc standards.

Pure drug and physical mixtures were heated from 25 to 130°C at a heating rate of 10°C /min, and held for 2 min. The samples were then cooled to −20°C at a cooling rate of 40°C /min, held for 2 min, and then heated again to 130 at 10°C /min. In the case of SDs, the samples were first equilibrated at −20°C for 2 min, and then heated to 130°C at a heating rate of 10°C /min.

Powder X-ray Diffraction (PXRD) Analysis

PXRD measurements were performed using a D/Max-2400 X-ray Fluorescence Spectrometer (Rigaku, Japan). A Cu Kα radiation anode tube was used at 56 kV 182 mA. Samples were scanned over a 2-theta range of 5–60° at a scan rate of 2°/min.

Fourier Transform Infrared (FTIR) Spectroscopy

FTIR spectra were obtained on a BRUKER EQUINOX55 FTIR spectrometer using the KBr disk method. The scans were performed over the wave number region of 4,000–400 cm^{-1} at a resolution of 2 cm^{-1}.

Raman Microscopy

Raman spectra of the pure CIN and Soluplus® were recorded using a Raman microscope (inVia, Renishaw, UK). The samples were irradiated with a 785 nm laser (laser power 150 mw) at room temperature. Raman mapping was performed on SDs to investigate the spatial distribution of the drug in SDs in a spectral range from 700 to 1,800 cm^{-1} in the StreamLine mode. A 50× objective lens was used and the step size was 5 μm in both the x and y directions.

Dissolution

The dissolution tests were performed using a paddle apparatus (ZRS-8G, Tianda Tianfa, China) according to the ChP (2010 Edition) at 37±0.5°C and 75 rpm. For CIN, a weak base, its solubility is dependent on the pH of the local environment. Hence the dissolution profiles of CIN-Soluplus® SDs will be significantly different from each other in dissolution media with different pH values. Herein, to discriminate between the dissolution behaviors of different formulations, several dissolution media of 900 mL with various pH values were used, including pH 4.5 acetate buffer (0.05 M), pH 6.8 phosphate buffer (0.05 M) and pH 7.6 phosphate buffer (0.05 M).

Samples equivalent to 25 mg drug were transferred into the dissolution vessel. 5 mL of dissolution samples were withdrawn at predetermined intervals, and passed through a 0.45 μm filter. The concentrations of CIN were subsequently quantified using a UV-photometer at a maximum wavelength of 253 nm. Analyses was carried out in triplicate. In addition, the particle size of the extrudates and the amorphous CIN used for the dissolution tests was in the range of 150–200 μm to allow comparison of the dissolution profiles of different formulations.

RESULTS

Construction of the Phase Diagram

As shown in Fig. 2, the temperature-composition phase diagram of CIN-Soluplus® SD was theoretically constructed based on the aforementioned methods, including the solubility curve, miscibility curve and T_g curve. The SDs in the region below the solubility curve are thermodynamically stable without the risk of phase separation or crystallization. However, for those above the miscibility curve, spontaneous phase separation will occur. The metastable region between the solubility and miscibility curves is divided into Zone I and II by the
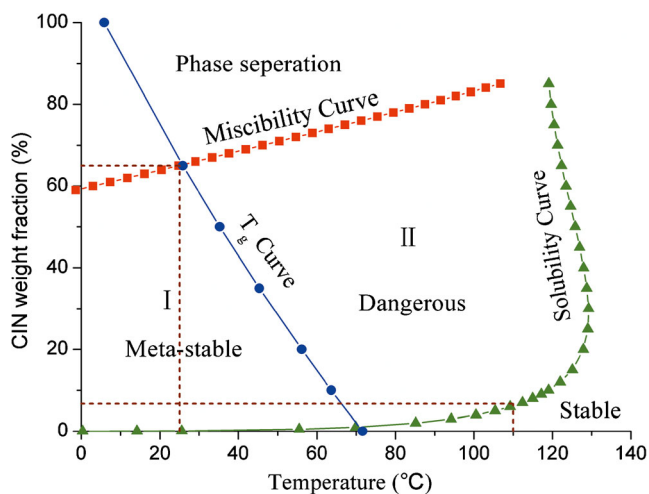
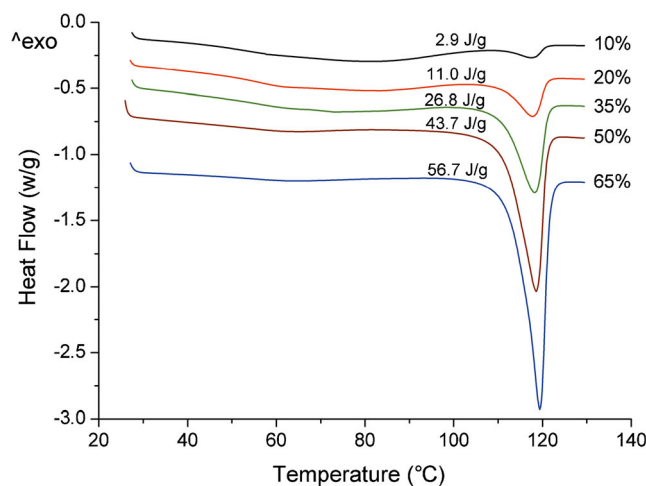**Fig. 2** Temperature–composition phase diagram predicted for the CIN-Soluplus® system.

Fig. 3 DSC thermograms of the first heating run for CIN/Soluplus® mixtures with 10, 20, 35, 50, and 65% w/w CIN from top to bottom.

T_g curve, and Zone I shares the potential to enhance both the drug loading and stability of SDs.

It can be seen from the phase diagram that the solubility and miscibility both increase with increasing the temperature, while T_g decreases with an increase in the drug weight fraction. According to the phase diagram, the solubility of CIN in Soluplus® is 0.1 wt% at 25°C and 6.3 wt% at 110°C, and the miscibility of CIN and Soluplus® is 65 wt% at 25°C. The predicted results indicate that CIN and Soluplus® could hardly form a solid solution and the maximum drug loading of SDs can not exceed 65 wt% at room temperature.

Solubility Measured by DSC

To verify the predicted solubility above, the solubility of CIN in Soluplus® was determined experimentally. The quantitative determination of the solubility of a crystalline drug in a polymer using DSC is based on the fact that a drug dissolved in the polymer will not be responsible for the enthalpy of fusion. Therefore, the solubility of a drug in a polymer can be estimated by plotting the enthalpy of fusion versus the drug concentration and making the extrapolation to zero enthalpy of fusion (25). DSC scans of the first heating run of CIN-Soluplus® physical mixtures with different drug concentrations are shown in Fig. 3. Each of the samples exhibited a single endothermic peak with a melting point (onset temperature) of 110°C. The enthalpy of fusion was plotted versus drug concentration and the regression equation was obtained using a linear regression model to fit the data (Fig. 4):

$$\Delta H = 1.00W - 7.93 \quad (r = 0.9985) \tag{12}$$

Where ΔH is the enthalpy of fusion, W is the weight fraction of CIN and r is the correlation coefficient of the regression line.

By extrapolating to zero enthalpy of fusion in Eq. (12), the solubility of CIN in Soluplus® was 7.9 wt%, calculated as the x-intercept of the regression line. It is worth noting that the solubility value provided here is that at the melting temperature of the drug (110°C) rather than at room temperature. Consequently, it could be assumed that the theoretically calculated solubility (6.3 wt%) is comparable with the measured one (7.9 wt%). Meanwhile, it was also demonstrated that for the CIN-Soluplus® system, the SLE equation can be used for estimation of the solubility curve.

Determination and Analysis of the T_g

CIN-Soluplus® SDs were formed after melting and rapid cooling of the physical mixtures using DSC as described in the **DSC Measurements** section. A second heating run was subsequently carried out to determine the T_g of SDs and the thermograms are presented in Fig. 5. All the SDs formed in
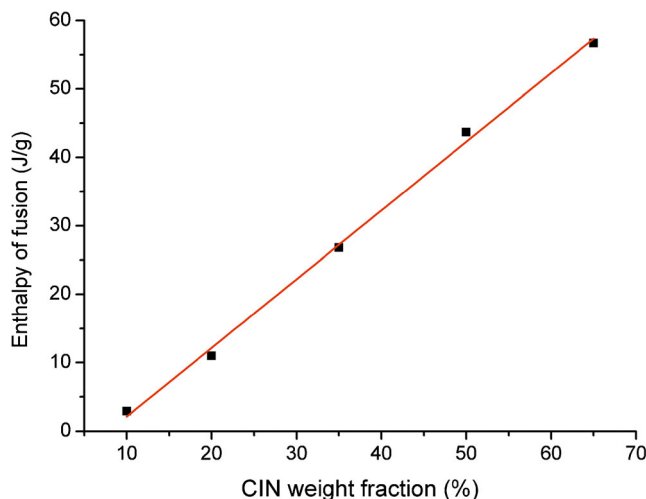

Fig. 4 Experimentally determined enthalpy of fusion as a function of the CIN concentration.
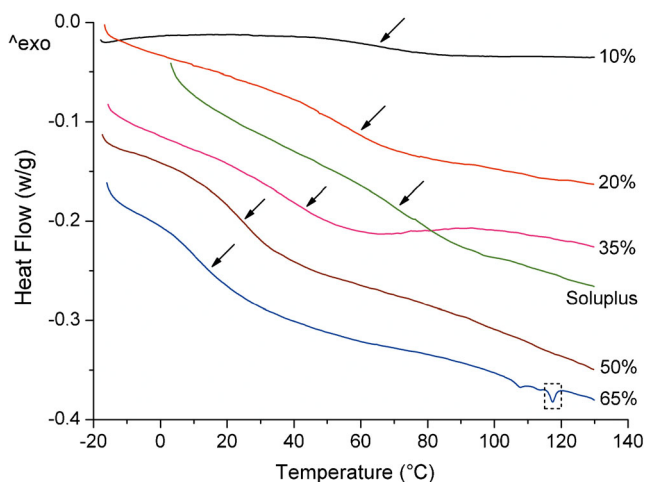
Fig. 5 DSC thermograms of Soluplus® and the second heating run for CIN/Soluplus® mixtures with 10, 20, 35, 50, and 65% w/w CIN. *Arrows* represent glass transition events.

Fig. 7 Compositional variation of the T_g for CIN/Soluplus® system experimentally determined or predicted by the Fox equation.

pans were amorphous exhibiting a single composition-dependent T_g between those of the two neat components except the sample with a CIN weight fraction of 65%, which also displayed a weak endothermic peak corresponding to the melting of crystalline CIN. Thermograms of the pure drug after the first and second heating are also shown in Fig. 6. The pure drug displayed a single melting point of 118.4°C during the first heating cycle, while during the second heating cycle, DSC scans of CIN revealed a T_g at 6°C. This was followed by an exothermic event in the range of 54~84°C and an endothermic peak at 115.2°C, due to the recrystallization of amorphous CIN and the melting of recrystallized CIN, respectively. DSC measurement was also performed on Soluplus®, which showed a T_g at 73°C.

Figure 7 shows the T_g of SDs determined using DSC together with the predicted T_g curve from the Fox equation. The T_gs of CIN and Soluplus® required for application of the Fox equation are 6 and 73°C respectively. By comparing the determined and predicted T_gs in Fig. 7, it can be seen that
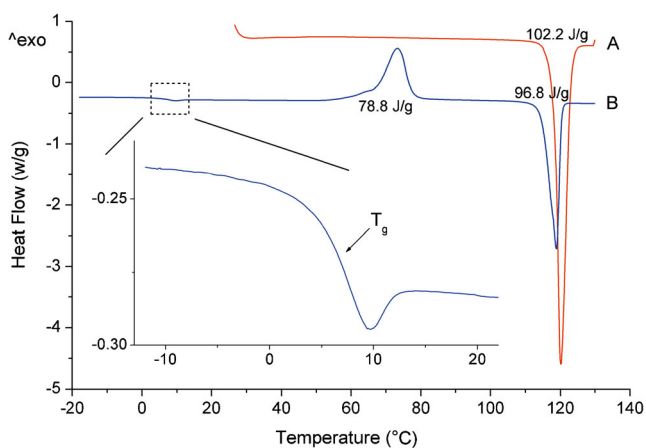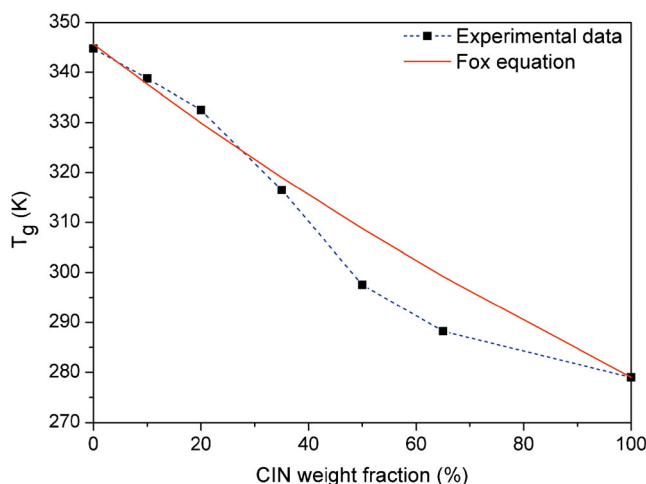
when the drug loadings are no more than 35 wt%, the experimental data fit the predicted ones well, while for higher drug loadings, a negative deviation was observed.

Determination of the Miscibility of CIN and Soluplus®

Compared with solubility and T_g, determination of the miscibility at a quantitative level is more challenging. So far there is no literature report of the direct experimental measurement of the miscibility of a drug and a polymer. As mentioned above, spontaneous phase separation takes place when the drug loading of SDs is higher than the miscibility at a certain temperature. Based on this theory, CIN-Soluplus® SDs with a series of drug loadings were prepared by hot melt extrusion, and the drug loading above which spontaneous phase separation occurred was investigated. By this means, the miscibility of CIN and Soluplus® was achieved.

In order to explore the phase separation, DSC measurements were first taken with freshly prepared SDs and the results are shown in Fig. 8. Division of the five thermograms
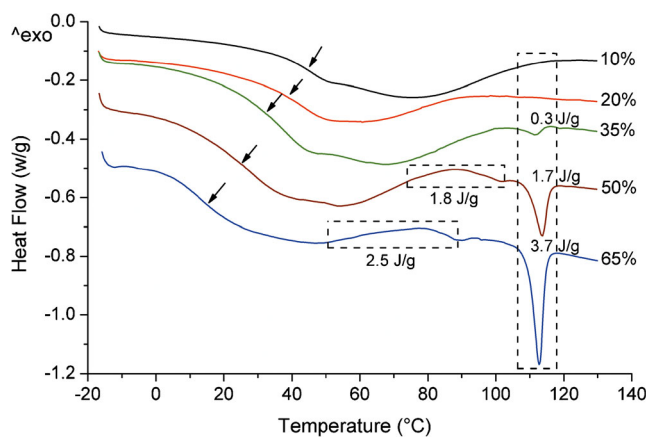

Fig. 6 DSC thermograms of the pure CIN after the first (**a**) and the second heating run (**b**).

Fig. 8 DSC thermograms of CIN-Soluplus® SDs with 10, 20, 35, 50, and 65% w/w CIN. *Arrows* represent glass transition events.

into two groups may be expected at first sight, because SD-10 and SD-20% presented only a single T_g. However, obvious endothermic peaks attributed to the melting of crystalline CIN were observed in SDs with higher drug loadings and the enthalpy of fusion rose with the increased drug loading. This appeared to indicate that a 35 wt% drug loading may be a critical value above which CIN molecules can crystallize out of the amorphous SDs, resulting in a spontaneous phase separation. However, PXRD results of SDs contradicted this assumption. It can been seen from Fig. 9 that the PXRD pattern of unprocessed CIN exhibits sharp Bragg peaks, characteristic of a crystalline material. In contrast, the diffractograms of Soluplus® and all SDs present only a diffuse halo with no Bragg peaks, characteristic of a PXRD amorphous system. This disagreement between DSC and PXRD led to a further examination of DSC thermograms. As a result, a broad exothermic peak was observed in SD-50 and SD-65% over the temperature range of 74~102 and 50~89°C respectively. This exotherm is located between the T_g and the melting endotherm, and can be attributed to the recrystallization of amorphous CIN. Subsequently, the amount of crystallized CIN contained in SDs expressed as a percentage of the total CIN was calculated from the enthalpies of recrystallization and fusion before and after the DSC scan. The results shown in Table II revealed a 6% crystallization for SD-65% after the DSC scan, together with a 1% crystallization that originally existed in freshly prepared SD and could not be detected by PXRD because of its extremely low concentration. It also indicated that 5% of CIN recrystallized during the DSC scan for SD-65% due to the heat. While for SD-50%, 4% crystallization was obtained, totally produced by recrystallization. In addition, the DSC thermogram of SD-35% displayed only a melting endothermic peak corresponding to a crystallization of 1%. Considering the detection limit of DSC, it was assumed that the exothermic peak of SD-35% was too weak to be detected, and the recrystallization was completely responsible for the crystallized CIN. Combining the DSC and PXRD results, it can be demonstrated that all the SDs were
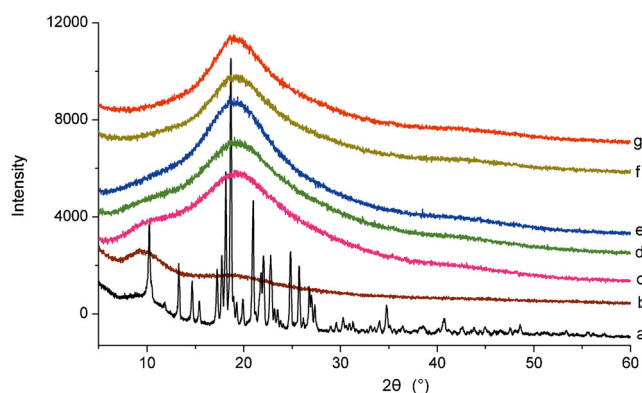

Fig. 9 PXRD patterns of CIN (**a**), Soluplus® (**b**), SD-10% (**c**), SD-20% (**d**), SD-35% (**e**), SD-50% (**f**), and SD-65% (**f**).

Table II Concentrations of Crystalline CIN for SD-35, SD-50 and SD-65% Before and After the DSC Scans

Crystalline CIN (%)	SD-35%	SD-50%	SD-65%
Before the DSC scans	0	0	1
After the DSC scans	1	4	6

amorphous except SD-65%, which contained an extremely low level of crystalline CIN, a sign of spontaneous phase separation. Based on these results, it appeared that the miscibility of CIN and Soluplus® is no more than 65 wt% at room temperature.

Dissolution Behavior of SDs

According to the analysis above, it can be seen that the miscibility experimentally determined is in agreement with that predicted by the phase diagram, which presented data of 65 wt% at 25°C. To further confirm the conclusion provided by DSC and PXRD, dissolution studies were performed on SDs. It is reasonable to assume that the dissolution behavior of SD-65% would be quite distinct from that of the others under certain dissolution conditions, if they really fall into different areas of the phase diagram. In fact, dissolution tests were first performed in 0.1 mol/L HCl (pH 1.0). It was found that the dissolution profiles of all SDs were no different from that of the pure crystalline CIN, because they all displayed complete dissolution at 15 min (data not shown). This is due to the very high solubility of CIN at pH 1.0 (solubility of CIN at pH 1.1 is 1.5 mg/mL (26)). So, dissolution tests were then conducted at a higher pH. The dissolution profiles of SDs in pH 4.5 acetate buffer were shown in Fig. 10a. For comparison, dissolution profiles of the crystalline and amorphous CIN were also given. It can be seen that dissolution rate of the amorphous CIN was enhanced compared with its crystalline counterpart, but it was still much slower than that of the SDs. The results also reveal that all SDs shared similar dissolution profiles except SD-65%, which demonstrated a much slower dissolution rate. This marked difference in dissolution between SD-65% and other SDs indicates that qualitative changes occurred to the form of the drug dispersed in SDs when the drug loading reached a level of 65 wt%. These results support the inference mentioned above, and agree with the predicted miscibility level at 25°C.

It has been shown that SD-65% is different from others with lower drug loadings, both in the form of drug dispersed in SDs and the dissolution behavior. Then one question deserving consideration is whether there is any difference in the dissolution behavior of SDs with drug loadings from 10 to 50%, although they are all amorphous. To investigate this issue, dissolution profiles were determined in pH 6.8 phosphate buffer first. The results obtained (Fig. 10b) showed that

SD-10 and SD-20% shared similar dissolution profiles under this condition. They both achieved a maximum dissolution of nearly 50% at 45 min, then followed by a rapid reduction in drug concentration. This phenomenon could be attributed to the high degree of supersaturation and precipitation of CIN, considering the very low solubility of CIN in the dissolution medium (solubility of CIN at pH 6.7 is 2.2 mg/L [26]). Compared with SD-10 and SD-20, SD-35% displayed an obvious decrease both in the rate and extent of dissolution. A maximum dissolution of about 30% was reached at 60 min, and then the concentration of CIN decreased slowly due to a low degree of supersaturation. In addition, under the dissolution testing conditions used, SD-50% exhibited the slowest dissolution rate and no decline in drug concentration was observed. Subsequently, dissolution tests were carried out in pH 7.6 phosphate buffer using SD-10 and SD-20%. As shown in Fig. 10c, fluctuating and irregular dissolution profiles were observed for both, because CIN was insoluble in pH 7.6 medium. Also, during the whole dissolution process, SD-10% maintained a higher extent of dissolution than SD-20%.

It can be seen from the dissolution studies that drug loading is a critical factor, which could directly affect the dissolution profiles of SDs. It is worth noting that for SDs with different drug loadings, a fully amorphous state is no guarantee of similar dissolution behavior. Drug would be released more easily from those with lower drug loadings.

FTIR Characterization

Possible interactions between CIN and Soluplus® in SDs were investigated by FTIR, as shown in Fig. 11. The spectrum of the physical mixture containing 20 wt% CIN showed a combination of pure CIN and pure Soluplus® with the same drug-polymer weight ratio. The spectrum of SD-20% was similar to that of the corresponding physical mixture except that some peaks arising from CIN became broader and merged to a large extent, indicating that CIN dispersed in SDs in amorphous form. Due to a lack of significant changes in wavenumber or relative intensity of peaks in SD-20%, it could be assumed that no specific interactions, such as hydrogen bonding, were exhibited by CIN and Soluplus®.

## DISCUSSION

Evaluation of the Predicted Phase Diagram

The solubility at 110°C and miscibility at 25°C of CIN in Soluplus® experimentally determined were 6.3 and 65 wt% respectively, both in good agreement with those provided by the phase diagram. Indeed, for the purpose of justifying the solubility at 25°C shown in the phase diagram (0.1 wt%), SD

with a drug loading of 5 wt% (SD-5%) was prepared by hot melt extrusion. Assuming that if the drug loading does not exceed the solubility of the drug in the polymer, the SD would be thermodynamically stable and retain its properties in any circumstances, dissolution tests were performed on SD-5% in pH 4.5 acetate buffer before and after exposure to 40°C and 75% relative humidity for 30 days. However, it was found that the rate and extent of dissolution decreased significantly after treatment (data not shown), indicating a thermodynamically unstable system for SD-5%. This demonstrated a low solubility of CIN in Soluplus®, at least no more than 5 wt%, thereby supporting the conclusion drawn from the phase diagram. Based on the results presented above, it can be assumed that information provided by the phase diagram agrees with the actual findings. So it is essential to explore the reasons for this, namely the applicability of the theories.

In the present work, the solubility curve was generated by the SLE equation, which needs information about the drug activity coefficient. Further, the F-H interaction parameter is required for calculation of the activity coefficient [11,12]. In addition, the F-H theory was used to determine the miscibility curve. According to this theory, the free energy of mixing is proposed to determine the miscibility of two species. It consists of two parts: entropy of mixing and enthalpy of mixing. The former always favours mixing, but the later can either promote or inhibit mixing. Generally, the entropy contribution to the free energy term is considered small and relatively constant, because the number of possible configurations of polymers is significantly reduced due to their large molecular weights. As a result, the enthalpic interactions determine whether the binary system is miscible or not. Similar to the activity coefficient, the enthalpic interactions also mainly depend on the interaction parameter. Consequently, the reliability of the phase diagram relies heavily on the accuracy of the interaction parameter.

According to literature reports, the melting point depression and solubility parameter are two methods widely used to estimate the interaction parameter for a drug-polymer system [11,27]. However, each method has its own limitations. It has been reported that complications can arise if experimentally determined melting point depression data is used to calculate the interaction parameter, because the melting point depression approach was developed from equilibrium conditions [28]. As a result, some measures were taken, such as reducing the particle size of materials and the scan rate of DSC, to maintain the phase equilibrium during heating [4]. Usually, the samples should be subjected to high energy milling to provide sufficient physical interaction between the drug and polymer, and also, a very low heating rate (1°C/min or even lower) is required to obtain the "true" melting point. Compared with melting point depression, the solubility parameter approach is simple and time-saving, because only a calculation based on the group contribution method is needed to

Fig. 10 Dissolution profiles of SD-10, SD-20, SD-35, SD-50 and SD-65% at pH 4.5 (**a**); Dissolution profiles of SD-10, SD-20, SD-35, and SD-50% at pH 6.8 (**b**); Dissolution profiles of SD-10 and SD-20% at pH 7.6 (**c**). Each point represents mean ± SD, $n = 3$.
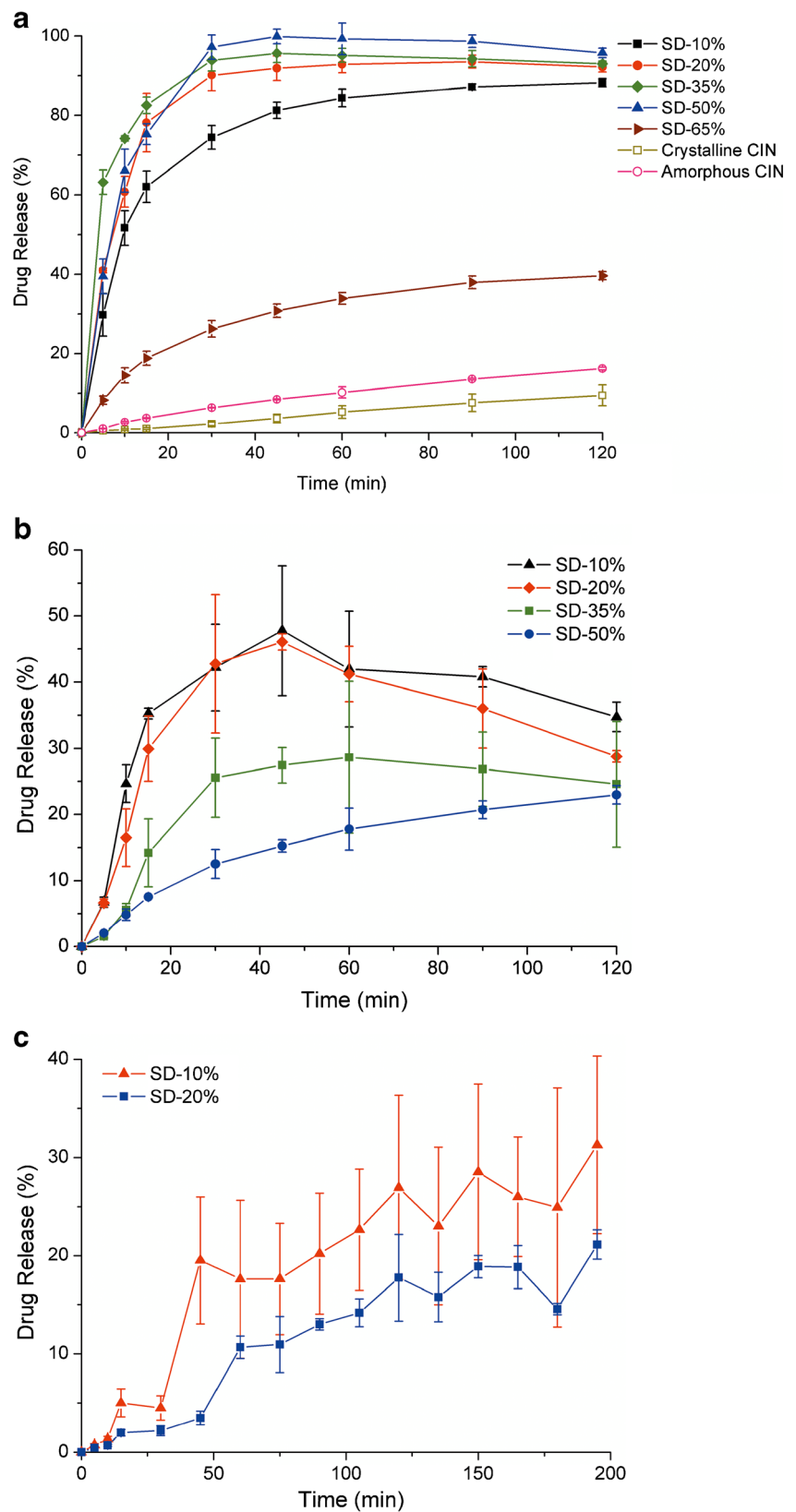
estimate the interaction parameter. However, this method is not applicable to systems that present specific interactions between the drug and polymer. In this work, the solubility parameter method was applied to calculate the interaction
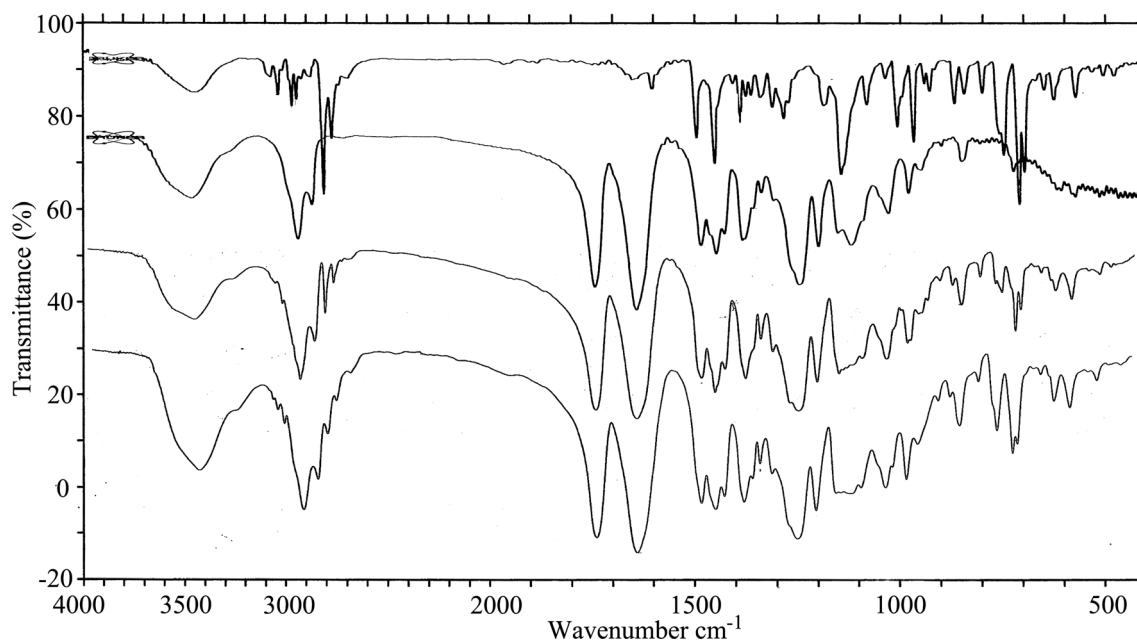
Fig. 11 FTIR spectra of CIN, Soluplus®, CIN/Soluplus® mixtures with 20 w/w CIN, and SD-20% from top to bottom.

parameter. Since the FTIR results have demonstrated the absence of specific interactions between CIN and Soluplus®, the solubility parameter method is suitable for this system. As a result, an interaction parameter in accordance with the practical situation was generated, leading to an acceptable phase diagram.

Forms of the Drug in Amorphous SDs

Generally, drugs can exist in polymers as molecular, amorphous or crystalline forms, depending on their solubility and miscibility in polymers and the drug loading of SDs. Here the amorphous form is defined as the agglomeration of drug molecules with disordered packing. The SDs would be thermodynamically stable when the drug is dispersed in a molecular or crystalline form. However, the amorphous form can generate a thermodynamically metastable system, which tends to crystallize. In practical terms, drugs can exist as a combination of two or three of these forms. Compared with the crystalline form, which can be identified readily by DSC or PXRD, it is difficult to distinguish between the molecular and amorphous forms, because they are both characterized by a non-crystalline state. Nevertheless, the solubility of a drug in a polymer is always too low to satisfy the dose requirement. So it is essential to investigate the properties of SDs with higher drug loadings.

The above studies have revealed an extremely low solubility (0.1 wt%) of CIN in Soluplus® at room temperature, so the drug molecules should not be dispersed uniformly throughout the SDs. To probing the spatial distribution of CIN in SDs, raman mapping was performed, and the results were shown in Fig. 12 presented in terms of peak intensity of CIN around

$1,000 \text{ cm}^{-1}$. As expected, it can be seen from these images that the drug distributed unevenly in all SDs to form drug-rich (red) and polymer-rich (dark blue) regions, leading to amorphous-amorphous phase separation. Moreover, the phase separated regions grew larger progressively with increased drug loading. These findings can explain the results of DSC. For SD-10 and SD-20% possessing low drug loadings, the size of drug-rich regions was small and the local drug concentration in these regions was relatively low. As a result, neither SD-10 nor SD-20% exhibited exothermic crystallization peak during the DSC scans. When the drug loading was increased to 35 wt%, the size of drug-rich regions increased significantly (Fig. 12d), indicating enhanced phase separation. The local drug concentration in these drug-rich regions should reach a critical value, because recrystallization occurred during the DSC heating, although the exothermic peak was not observed. For SD-50 and 65%, the drug loading was increased further, leading to drug-rich regions with larger dimensions. Due to the high drug concentration in these drug-rich regions, recrystallization could take place easily during the DSC scans, as reflected by the obvious exothermic crystallization peak. In addition, more information can be obtained from the recrystallization temperature range of SD-50 and SD-65%. As shown in Figs. 6 and 8, the recrystallization temperature range of SD-50% (74~102°C) was higher than that of the pure amorphous CIN (54~84°C). This indicates that some polymers still remained in drug-rich regions of SD-50%, which could hinder the recrystallization of drug molecules to some extent. In contrast, the recrystallization temperature range of SD-65% (50~89°C) was similar to that of the pure amorphous CIN. This strongly suggests that drug-rich regions in SD-65% have completely phase separated, and
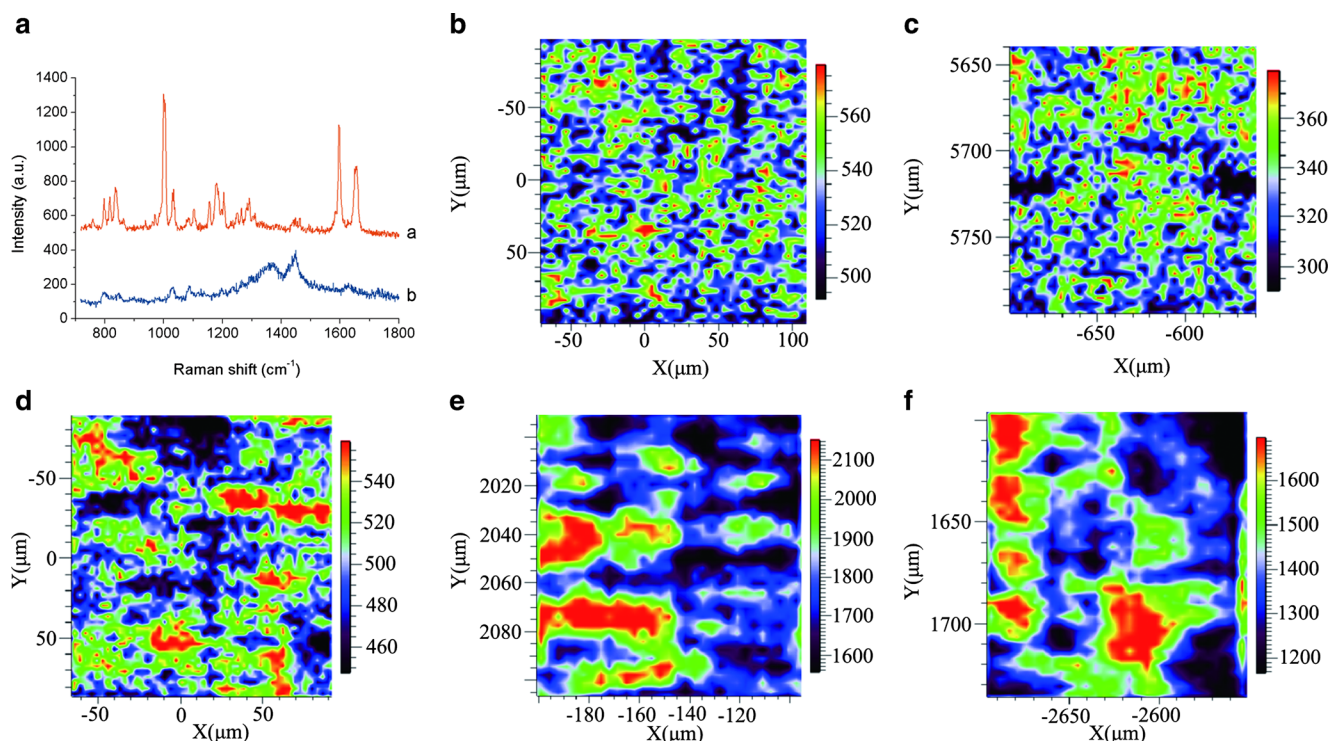
Fig. 12 Raman spectra of pure (**a**) CIN and (**b**) Soluplus (**a**), and XY raman mapping of SD-10% (**b**), SD-20% (**c**), SD-35% (**d**), SD-50% (**e**) and SD-65% (**f**). Color bars indicate the intensity of CIN characteristic peak (~1,000 cm^{-1}). Red color represents higher concentration of CIN.

pure amorphous drug domains without any polymers have been generated. In addition, the raman data also indicate that dissolution of SDs is correlated with the forms of the drug in SDs. As shown in this study, phase separation has an adverse effect on the dissolution of SDs. Those possessing drug-rich regions with large dimension and high local drug concentration will show poor dissolution.

Mixing Level between CIN and Soluplus®

It has been widely reported that the T_g of a mixture can be related to the T_gs of its components by some equations (6). The relationship between the T_g and composition can reflect interactions or the mixing level of a drug-polymer system. It is assumed that the goodness of fit of the experimental data to the equation indicates an ideal mixing of two components. However, deviations from ideal behavior can always be observed and explained by differences in the strength of intermolecular interactions between individual components and those of the blend. Usually, the presence of strong interactions between the drug and polymer will lead to a positive deviation (i.e. the T_g measured is higher than the predicted value), and a negative deviation can occur when the drug and polymer bind less strongly to each other than to themselves (29). For the CIN-Soluplus® system, due to the absence of a specific drug-polymer interaction revealed by FTIR, and a positive interaction parameter (0.76) calculated from the solubility

parameter, it can be inferred that drug-drug interactions are stronger than that of the drug-polymer. Hence, negative deviations should be generated. However, as shown in Fig. 7, ideal behavior was observed for the CIN-Soluplus® mixture with a drug weight fraction no more than 35%, suggesting that the drug was uniformly dispersed throughout the blend to produce mixing at a molecular level. This disagreement suggests that the observed ideal mixing is a result of the solid solution formed at a high temperature and kinetically frozen during the cooling process, rather than a thermodynamic equilibrium. If this is the case, increasing the ratio of the drug in mixtures would lead to a self-association of drug molecules, due to stronger interactions between them and decreased concentrations of the polymer, and as a result, negative deviations could be observed. As can be seen from Fig. 7, the systems with a drug weight fraction of 50 and 65% both displayed negative deviations, and even a weak endothermic peak appeared at the temperature corresponding to the melting of crystalline CIN for the sample with a 65% drug weight fraction (Fig. 5), although it is unclear whether they were generated during the cooling process or caused by recrystallization in the second heating circle. These results suggest the influence of interactions between the drug and polymer on the mixing level of these two components.

CONCLUSION

This work shows how to construct a phase diagram of SDs using a theoretical approach, according to the SLE equation, the F-H theory and the Fox equation. Using CIN-Soluplus® SD as a model system, the predicted phase diagram was evaluated by comparing the solubility, miscibility and T_g experimentally determined with those predicted by the phase diagram. It was found that the key to the reliability of the phase diagram depends on the accuracy of the interaction parameter, and also, it is reasonable to estimate the interaction parameter using the solubility parameter approach for non-polar mixtures interacting mainly by dispersion forces. The interaction parameter can determine the intermolecular interactions between the drug and polymer, thus markedly influencing the mixing level between the drug and polymer. It should be emphasized that a fully amorphous state is no guarantee of similar properties for SDs. The forms of the drug dispersed in polymers and the dissolution behavior could be significantly different for SDs possessing completely an amorphous state but different drug loadings. In addition, the appearance of crystalline drug might adversely affect SDs in spite of an extremely low concentration.

REFERENCES

1. Alam MA, Ali R, Al-Jenoobi FI, Al-Mohizea AM. Solid dispersions: a strategy for poorly aqueous soluble drugs and technology updates. Expert Opin Drug Deliv. 2012;9(11):1419–40.
2. Qian F, Huang J, Hussain MA. Drug–polymer solubility and miscibility: stability consideration and practical challenges in amorphous solid dispersion development. J Pharm Sci. 2010;99(7):2941–7.
3. Zhao Y, Inbar P, Chokshi HP, Malick AW, Choi DS. Prediction of the thermal phase diagram of amorphous solid dispersions by Flory–Huggins theory. J Pharm Sci. 2011;100(8):3196–207.
4. Tao J, Sun Y, Zhang GG, Yu L. Solubility of small-molecule crystals in polymers: d-mannitol in PVP, indomethacin in PVP/VA, and nifedipine in PVP/VA. Pharm Res. 2009;26(4):855–64.
5. Karavas E, Georgarakis M, Docoslis A, Bikiaris D. Combining SEM, TEM, and micro-Raman techniques to differentiate between the amorphous molecular level dispersions and nanodispersions of a poorly water-soluble drug within a polymer matrix. Int J Pharm. 2007;340(1):76–83.
6. A.M. Kaushal, P. Gupta, and A.K. Bansal. Amorphous drug delivery systems: molecular aspects, design, and performance. Critical Reviews™ in Ther Drug Carrier Syst. 2004;21(3).
7. Greco S, Authelin J-R, Leveder C, Segalini A. A practical method to predict physical stability of amorphous solid dispersions. Pharm Res. 2012;29(10):2792–805.
8. Linand D, Huang Y. A thermal analysis method to predict the complete phase diagram of drug–polymer solid dispersions. Int J Pharm. 2010;399(1):109–15.
9. Sun Y, Tao J, Zhang GG, Yu L. Solubilities of crystalline drugs in polymers: an improved analytical method and comparison of solubilities of indomethacin and nifedipine in PVP, PVP/VA, and PVAc. J Pharm Sci. 2010;99(9):4023–31.
10. Mahieu A, Willart J-F, Dudognon E, Danède F, Descamps M. A new protocol to determine the solubility of drugs into polymer matrixes. Mol Pharm. 2013;10(2):560–6.
11. Marsac PJ, Shamblin SL, Taylor LS. Theoretical and practical approaches for prediction of drug–polymer miscibility and solubility. Pharm Res. 2006;23(10):2417–26.
12. Marsac PJ, Li T, Taylor LS. Estimation of drug–polymer miscibility and solubility in amorphous solid dispersions using experimentally determined interaction parameters. Pharm Res. 2009;26(1):139–51.
13. Bellantone RA, Patel P, Sandhu H, Choi DS, Singhal D, Chokshi H, et al. A method to predict the equilibrium solubility of drugs in solid polymers near room temperature using thermal analysis. J Pharm Sci. 2012;101(12):4549–58.
14. M. Rubinsteinand R.H. Colby. Polymer physics, OUP Oxford; 2003.
15. S.Z. Cheng. Phase transitions in polymers: the role of metastable states: the role of metastable states, Elsevier; 2008.
16. Kalogerasand IM, Brostow W. Glass transition temperatures in binary polymer blends. J Polym Sci B. 2009;47(1):80–95.
17. Jayachandra Babu R, Brostow W, Kalogeras IM, Sathigari S. Glass transitions in binary drug + polymer systems. Mater Lett. 2009;63(30):2666–8.
18. Kalogeras IM. A novel approach for analyzing glass-transition temperature vs. composition patterns: application to pharmaceutical compound + polymer systems. Eur J Pharm Sci. 2011;42(5):470–83.
19. A. Chan, K. Coppens, M. Hall, V. He, P. Jog, P. Larsen, B. Koblinksi, M. Read, D. Rothe, and S. Somasi. Solubility parameters as a tool to predict API morphology in hot melt extruded (HME) formulations containing ethycellulose, hypromellose, and polyethylene oxide, 2006 Am Assoc Pharm Sci Annu Meet Expo, San Antonio, TX, Vol. 29,2006.
20. Djuris J, Nikolakakis I, Ibric S, Djuric Z, Kachrimanis K. Preparation of carbamazepine–Soluplus® solid dispersions by hot-melt extrusion, and prediction of drug–polymer miscibility by thermodynamic model fitting. Eur J Pharm Biopharm. 2013;84(1):228–37.
21. Frankand TC, Gupta S. Quickly screen solvents for organic solids. Chem Eng Prog. 1999;95(12):41–61.
22. Van Eerdenbrugh B, Vermant J, Martens JA, Froyen L, Van Humbeeck J, Augustijns P, et al. A screening study of surface stabilization during the production of drug nanocrystals. J Pharm Sci. 2009;98(6):2091–103.
23. Forster A, Hempenstall J, Tucker I, Rades T. Selection of excipients for melt extrusion with two poorly water-soluble drugs by solubility parameter calculation and thermal analysis. Int J Pharm. 2001;226(1):147–61.
24. Fox T. Influence of diluent and of copolymer composition on the glass temperature of a polymer system. Bull Am Phys Soc. 1956;1(123):22060–6218.
25. Gramaglia D, Conway BR, Kett VL, Malcolm RK, Batchelor HK. High speed DSC (hyper-DSC) as a tool to measure the solubility of a drug within a solid or semi-solid matrix. Int J Pharm. 2005;301(1):1–5.
26. Ogata H, Aoyagi N, Kaniwa N, Ejima A, Sekine N, Kitamura M, et al. Gastric acidity dependent bioavailability of cinnarizine from two commercial capsules in healthy volunteers. Int J Pharm. 1986;29(2):113–20.
27. Tian Y, Booth J, Meehan E, Jones DS, Li S, Andrews GP. Construction of drug–polymer thermodynamic phase diagrams using Flory–Huggins interaction theory: identifying the relevance of temperature and drug weight fraction to phase separation within solid dispersions. Mol Pharm. 2012;10(1):236–48.
28. Rimand PB, Runt JP. Melting point depression in crystalline/compatible polymer blends. Macromolecules. 1984;17(8):1520–6.
29. Nair R, Nyamweya N, Gönen S, Martınez-Miranda L, Hoag S. Influence of various drugs on the glass transition temperature of poly(vinylpyrrolidone): a thermodynamic and spectroscopic investigation. Int J Pharm. 2001;225(1):83–96.